Draft version April 23, 2024
Typeset using LaTeX **twocolumn** style in AASTeX631

Open Cluster Dynamics under the Influence of Outflow-Ambient Interactions

Muxin Liu [1,2] Lile Wang [2,1,*] Xiaoting Fu [3] and Luis C. Ho [2,1]

[1] Department of Astronomy, School of Physics, Peking University, Beijing 100871, China
[2] Kavli Institute for Astronomy and Astrophysics, Peking University, Beijing 100871, China
[3] Purple Mountain Observatory, Chinese Academy of Sciences, Nanjing 210023, China

ABSTRACT

Outflowing stars impinging upon ambient gas experience accelerations due to the gravitational feedback from the morphology of the interaction betweem the outflow and the ambient gas. Such "negative dynamical friction" (NDF), in contrast to the conventional "dynamical friction" (DF), is studied for its impact on the dynamics of open clusters immersed in a uniform ambient gas. We modify the N-body integration code `REBOUND` with both NDF and DF implemented according to the outflow conditions of each star in a consistently constructed model open cluster. The evolution of stars is also involved in determining the gas-star interactions throughout their stellar lives. Compared to DF-only and gas-free models with identical initial conditions, the NDF-affected cluster is puffier and evaporates faster, as indicated by various diagnostics, including lower velocity dispersions and larger half-mass and half-light radii. Neutron stars with fast winds are expelled from the cluster due to their intensive NDF effect, even without the "kicks" by asymmetric supernovae. Exploration of parameter space confirms that the NDF effect is generally enhanced with higher ambient gas densities, in qualitatively agreement with the expression of acceleration. Outflow-ambient interactions should be considered for the proper interpretation of the evolution of stellar dynamics in clusters.

Keywords: Open star clusters (1160), Stellar dynamics (1596), Stellar winds (1636), Stellar mass loss (1613), Dynamical friction (422), Neutron stars (1108), N-body simulations (1083)

1. INTRODUCTION

Open clusters (OCs) offer valuable insights into the formation and evolution of stars. Comprised of approximately 10^2 to 10^4 stars that are gravitationally bound to each other (Binney & Tremaine 2008), OCs comprise well-defined single stellar populations. They form from the collapse of a common molecular cloud (Krumholz et al. 2019), with the same metallicity and age. As a result, OCs serve as valuable tracers of star formation, chemical evolution, kinematics, and gravitational dynamics (see, e.g., Friel 1995; Krumholz et al. 2019; Cantat-Gaudin 2022; Fu et al. 2022; Magrini et al. 2023). For instance, they can be utilized to determine the metallicity of stellar populations in different regions of the Milky Way, as their distances can be constrained by their color-magnitude diagrams (see, e.g., Sandage 1953). Moreover, the kinematic properties of OCs can be used to trace the rotation curve of the Milky Way (see, e.g., Tarricq et al. 2021). Thanks to the contributions of missions like Gaia (Gaia Collaboration et al. 2016) in providing stellar astrometry information, including precise position, parallax, and proper motion, significant advancements have been made (e.g., Gaia Collaboration et al. 2018, 2021, 2023). The member stars of OCs and the properties of several thousand clusters have been determined based on Gaia data (see, e.g., Cantat-Gaudin 2022; Hunt & Reffert 2023). Some OCs show tidal structures and indicate interactions with their environments (see, e.g., Pang et al. 2022; Tarricq et al. 2022). These advancements enable the study of the dynamical characteristics of OCs through observations and facilitate comparison with theoretical models.

Most Galactic OCs travel in the Milky Way thin disk on non-circular orbits that pass through the Galactic mid-plane several times in one orbital revolution (see, e.g., Fu et al. 2022). The impact of the detailed interactions between the cluster member stars and the gas clouds in the Galactic plane remains unclear. Do the interactions change the morphology of the star clusters and lead to the loss of member stars? Do the interac-

* E-mail: lilew@pku.edu.cn

tions differ among different kinds of stars? These are still open questions.

The ambient gas density likely will affect the dynamical characteristics of an OC as it travels through a gas cloud. A massive object moving through a giant gas cloud experiences dynamic friction (DF) (Chandrasekhar 1943; Ostriker 1999; Edgar 2004). According to the standard Bondi-Hoyle-Lyttleton accretion model (Hoyle & Lyttleton 1939; Bondi & Hoyle 1944; Edgar 2004), it is understood that due to the long-range nature of gravity, the gas outside the Bondi radius is also influenced by gravity, resulting in the formation of an overdense tail downstream of the massive object. This overdense region exerts a pulling force on the object in the opposite direction of its motion, causing it to decelerate. This force is known as DF force. Works such as Kim & Kim (2007) and Baruteau et al. (2011) have shown that gas DF can lead to the hardening of binaries, and Tagawa et al. (2020) have pointed out that binaries can form through single-single interactions by dissipating kinetic energy in a gaseous medium. Other works, such as Tanaka et al. (2002), have shown that DF force can dampen the velocity dispersion of black holes (BHs) and stars, and Just et al. (2012) have demonstrated that this dissipative force acting on stars in the disk can result in an increased mass flow toward the supermassive BH and an asymmetry in the phase space distribution due to a rotating accretion disk.

However, the situation changes if stellar objects launch powerful winds. Gruzinov et al. (2020) demonstrated that when the wind speed is sufficiently high, the extent of the underdense region becomes substantial, resulting in an overall gravitational force from the gas that aligns with the object's motion. Consequently, the DF becomes negative in this scenario, causing the object to accelerate. This phenomenon is known as negative dynamic friction (NDF). In other related works, Li et al. (2020) employed hydrodynamic simulations to explore the changes in accretion rate and the strength of NDF in the presence of outflows from compact objects. Additionally, Wang & Li (2022) conducted a study on NDF in the context of a binary system using global 3D hydrodynamic simulations. This work uses the N-body integrator `REBOUND` (Rein & Liu 2012) to study the impact of NDF on the dynamics of OCs immersed in a uniform ambient gas. Thanks to the support of `REBOUND` in allowing the incorporation of additional physics, both NDF and DF are implemented according to the outflow conditions of each star in a model OC that is consistently constructed.

This paper is structured as follows. Section 2 provides comprehensive descriptions of the gas-star interactions incorporated, the stellar evolution model, and the setup of the fiducial model. Section 3 analyzes and compares the impacts of different types of gas-star interactions—namely, DF, NDF, and "None"—on the dynamics and stellar evolution of the fiducial model OC, both with and without bulk motion. Section 4 explores scenarios with various ambient gas densities. Discussion and a summary are given in Section 5.

2. METHODS

This work simulates the dynamics of gas-coupled OCs using N-body simulations by adding modules to `REBOUND`. For accuracy, we adopt the `IAS15` integrator (Rein & Spiegel 2015), which is a 15th order scheme with adaptive step size control. In order to model the clusters properly, stellar particles are created with proper mass distributions and evolved with stellar evolution models that include compact objects epochs along with the dynamics.

2.1. *Gas-star Interactions*

The interaction between gas and stars can generate either friction or anti-friction, depending on the strength of the stellar outflows. For stars that have no outflows, the analytic approximations for dynamical friction are adopted from Ostriker (1999):

$$a_{\rm DF} = \frac{4\pi G^2\rho}{v_*^2} \times \begin{cases} \ln\left[\Lambda\left(1-\dfrac{1}{\mathcal{M}^2}\right)^{1/2}\right] , & \mathcal{M}>1 \\ \dfrac{1}{2}\ln\left(\dfrac{1+\mathcal{M}}{1-\mathcal{M}}\right)-\mathcal{M} , & \mathcal{M}<1 , \end{cases} \tag{1}$$

where v_* is the star's velocity, $\mathcal{M} \equiv v_*/c_s$ is the Mach number in the gas, and $\Lambda \equiv b_{\rm max}/b_{\rm min}$ is the Coulomb factor. We use the Bondi radius of each star, $b_{\rm min} \equiv 2GM/c_s^2$, for the minimum impact parameter, and we approximate $b_{\rm max}$ with the size upper limit of a giant molecular cloud ($\sim$ 100 pc in this work; e.g., Solomon et al. 1987; Miville-Deschênes et al. 2017; Sun et al. 2018)

Whenever a star has outflows, the gravitational feedback coming from the interactions between such outflows and the ambient gas will likely accelerate the star. We adopt the analytic approximation described in Gruzinov et al. (2020) and Li et al. (2020),

$$a_{\rm NDF} \simeq \pi G\rho_0 \int_0^\pi {\rm d}\theta\ \cos\theta\sin\theta\ R_s \times \left\{\frac{3}{2}\left[1+\frac{2u(1-\cos\theta)}{R_s^2\sin^2\theta/R_0^2}\right]^2 - 2\left[1+\frac{u^2}{R_s^2/R_0^2}\right]\right\} , \tag{2}$$

where $R_0 = [\dot{m}_{\rm w} v_{\rm w}/(4\pi\rho_0 v_*^2)]^{1/2}$ is the standoff distance (where the total pressure of the incoming medium equals to that of the outflow), $\dot{m}_{\rm w}$ is the outflow wind mass-loss rate, v_w is the wind radial velocity, $R_s \simeq R_0[3(1-\theta\cot\theta)/\sin^2\theta]^{1/2}$ is the location of the contact discontinuity at the polar angle θ (where the gas overdensities ae located), and $u \equiv v_*/v_{\rm w}$. In general, for typical OCs, $v_* \lesssim 1-10$ km s^{-1} (Tarricq et al. 2021), which is significantly lower than the $v_{\rm w}$ of almost all stellar outflows. Even asymptotic giant branch (AGB) stars, which are known for their slow outflows, still have $v_{\rm w} \gtrsim 30$ km s^{-1} (Habing & Olofsson 2004; Ramstedt et al. 2008). Therefore, one can take the $u \to 0$ limit of Eq. (2) and adopt a simple analytic approximation, $a_{\rm NDF} \simeq 8.18 G\rho_0 R_0$ (see also Li et al. 2020).

There are multiple types of stars in an OC, and their interactions with the ambient gas are different. Unless otherwise noted, we use the anti-friction recipes for main sequence stars, red giant branch (RGB) stars, and neutron stars (NSs), while we assume that white dwarfs (WDs) and BHs have *no* outflows and thus obey $a_{\rm DF}$ in Eq. (1). Admittedly, WDs and BHs in binaries can accrete and have consequent activities (e.g., disk winds, decretions, and jets), yet detailed discussions on those phenomena only add to the complications and obscure the effects concerned, and are beyond the scope of the current paper. For main sequence stars and giants, the wind properties are calibrated for stars with solar metallicity. The mass-loss rates are approximated by Reimers formula (e.g., Kudritzki & Reimers 1978; see also Choi et al. 2016),

$$\begin{aligned}\dot{m}_{\rm w} &\simeq 4\times10^{-13}\ M_\odot\ {\rm yr}^{-1} \times \left(\frac{L}{L_\odot}\right)\left(\frac{R}{R_\odot}\right)\left(\frac{M}{M_\odot}\right)^{-1} \\ &\sim 4\times10^{-13}\ M_\odot\ {\rm yr}^{-1} \times \left(\frac{M}{M_\odot}\right)^{3.3} ,\end{aligned} \tag{3}$$

where we use the approximate scaling laws $L \propto M^{3.5}$ (Kuiper 1938) and $R \propto M^{0.8}$ (Demircan & Kahraman 1991). Such mass-loss rates are on the high end of typical values, yet stars in an OC are generally young and tend to have stronger stellar winds. The stellar wind velocity has significant variations and uncertainties from star to star. We adopt a simplified power-law fitting for main sequence stars,

$$v_w \simeq 400\ {\rm km\ s}^{-1} \times \left(\frac{M}{M_\odot}\right)^{0.6} , \tag{4}$$

which yields observed values of $v_w \simeq 400$ km s^{-1} for solar-mass stars (e.g., Brooks et al. 2015), and $v_w \simeq 2000$ km s^{-1} for type O8 stars (e.g., Bernabeu et al. 1989). The uncertainties of wind properties are even greater for RGB stars; for simplicity, we assume all of them have $v_{\rm w,RGB} \simeq 30$ km s^{-1} and $\dot{m}_{\rm w,RGB} \simeq 3\times10^{-9}\ M_\odot$ yr^{-1} (Habing & Olofsson 2004; Ramstedt et al. 2008). Neutron stars can have significant outflows due to complex acceleration mechanisms (such as winds originating from young and intensely hot neutron stars are propelled by the absorption of high-energy neutrinos by photons and neutrons near the stellar surface (Salpeter & Shapiro 1981; Duncan et al. 1986)), and we assume $v_w \simeq 3\times10^4$ km s$^{-1} \simeq 0.1c$ (c for the speed of light), and $\dot{m}_{\rm w} \simeq 3\times10^{-9}\ M_\odot$ yr^{-1} (e.g., Kato 1983; Paczynski 1990; Mor et al. 2023).

2.2. *Stellar Evolution Properties*

Stars in an OC evolve for hundreds of millions of years before the cluster evaporates (Portegies Zwart et al. 2010; Krumholz et al. 2019; Krause et al. 2020). Given that the main sequence lifetime of an 8 $M_\odot$ star with solar metallicity is about 35 Myr (see stellar model `PARSEC v1.2s`; [1] Bressan et al. 2012; Tang et al. 2014; Chen et al. 2015), before the cluster evaporates all massive stars will have evolved off the main sequence. Very massive stars ($M \gtrsim 25\ M_\odot$) are not considered in this work. We assume that each star has finished its main sequence phase and entered its RGB stage at the time we consider significant gas-star interactions to occur. The evolution time of the RGB phase is approximated by a piecewise function in line with the solar metallicity and solar composition stellar models (Z=0.017, Y=0.279) of `PARSEC v1.2s`:

$$t_{\rm RGB} = \begin{cases} 10^5\ {\rm yr}\ ,\ M > 15\ M_\odot \\ 3\times10^8 \times \left(\frac{M}{M_\odot}\right)^{-4}\ {\rm yr}\ ,\ M \le 15\ M_\odot\ . \end{cases} \tag{5}$$

After the RGB stage, we assume that stars of $M < 8\ M_\odot$ will undergo their AGB phase and end up as WDs. Because the AGB stage experiences massive outflows that lose $\sim 50\%$ of the stellar mass within a relatively short period ($\Delta t \lesssim 10^5$ yr), the impact of AGB outflows due to anti-friction can be accounted as a pulse momentum injection, by integrating ${\rm d}v/{\rm d}t = a_{\rm NDF}$ assuming $u \ll 1$

[1] https://people.sissa.it/∼sbressan/parsec.html

and $\dot{m}_{\rm w} \simeq \Delta M/\Delta t$,

$$\begin{aligned}\Delta|v^2| &\simeq 2\int_0^{\Delta t} a_{\rm NDF} v\ {\rm d}t \\ &\simeq 3\times10^{-2}\ {\rm km}^2\ {\rm s}^{-2} \times \left(\frac{\rho}{30\ m_p\ {\rm cm}^{-3}}\right)^{1/2} \\ &\times \left(\frac{\Delta M}{M_\odot}\right)^{1/2} \left(\frac{v_{\rm w}}{30\ {\rm km\ s}^{-1}}\right)^{1/2} \left(\frac{\Delta t}{10^5\ {\rm yr}}\right)^{1/2},\end{aligned} \tag{6}$$

where m_p is the proton mass and ΔM is the total mass-loss during the period. We assume that the consequent WD has $M_{\rm WD} \simeq \min\{0.5M, M_\odot\}$ (here M is for the progenitor RGB star mass), and ΔM is given by the decrease of mass before becoming a WD. For stars with $M > 8\ M_\odot$, we estimate their $\Delta|v^2|$ similarly, assuming that the expansion period of the supernova ejecta is $\Delta t \sim 10^4$ yr, $v_{\rm w} \simeq 0.1c$, and ΔM is also deduced from $M_{\rm NS} \simeq \min\{0.1M, 1.5M_\odot\}$ and the progenitor mass M. Note that we intentionally ignore the "kicks" in NS momenta induced by the asymmetries of supernovae, so as not to obscure the NDF by the uncertainty of such kicks (actually NDF only adds to the effects of the kicks). Other epochs of stellar evolution are ignored as they have negligible impact on the stellar cluster dynamics.

2.3. *Setup of Fiducial and Other Models*

The fiducial model studies an OC immersed in the cold neutral medium (CNM) in the Galaxy, which has $\rho \simeq 30\ m_p\ {\rm cm}^{-3}$ and $T \simeq 100$ K (Draine 2011). The initial condition is set using a two-phase method. The first phase generates an ensemble of 2000 stars using the broken power-law initial mass function over the stellar mass range $0.2 < (M/M_\odot) < 25$ (Kroupa 2002),

$$\xi(M) \propto \begin{cases} M^{-2.35}\ , & M > M_\odot \\ M^{-1.3}\ , & M < M_\odot\ . \end{cases} \tag{7}$$

At the beginning of this phase, all stars have zero velocity and are distributed uniformly within an $r < 1$ pc sphere. In the second phase, this initial ensemble of stars is evolved using `REBOUND` *without* any stellar evolution processes or interactions with gas through 100 Myr, which is about twice as long as the relaxation timescale (ΣM is the total mass, and $R_{\rm oc}$ is the approximate size of the OC),

$$\begin{aligned} t_{\rm relax} &\sim \left(\frac{0.1N}{\ln N}\right) \times t_{\rm cross}\ , \\ t_{\rm cross} &\sim \left(\frac{R_{\rm oc}^3}{G\ \Sigma M}\right)^{1/2} \\ &\sim 4\ {\rm Myr} \times \left(\frac{\Sigma M}{2\times10^3\ M_\odot}\right)^{-1/2} \left(\frac{R_{\rm oc}}{5\ {\rm pc}}\right)^{3/2}. \end{aligned} \tag{8}$$

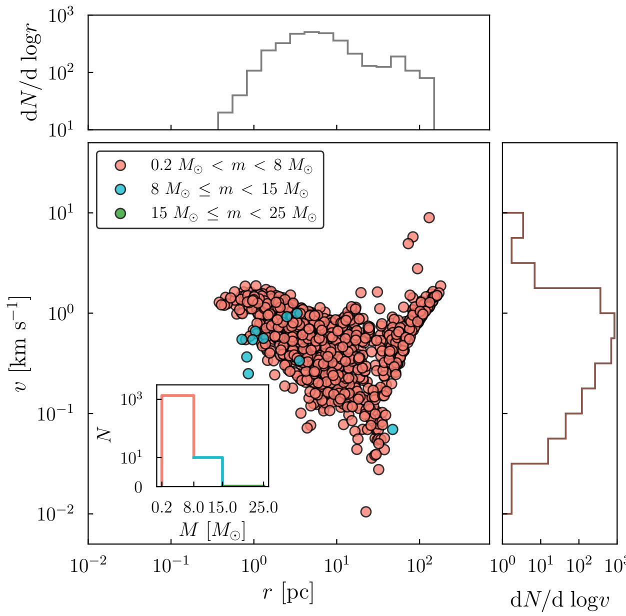

Figure 1. The initial condition of the fiducial model includes logarithmic density histograms of distance (to the cluster center) and velocity in the upper and right panels, respectively. Note that the histograms of distances and velocities are calculated with respect to the median value. In the scatter plot, different colors represent different mass ranges, revealing the absence of stars with $M \geq 15\ M_\odot$ (1357 stars falling into the smallest mass range, 10 in the middle mass range). The velocity dispersion for this sample is ~ 0.69 km s^{-1}.

After this phase, 1367 stars with a total mass $\Sigma M = 1233.7\ M_\odot$ are left within the 200 pc bounding box (see Figures 1–2), and the evolution times of all the remaining stars are reset to zero. The consequent star ensemble is then adopted as the initial condition of the fiducial simulation, which is then evolved for $\Delta t_{\rm evo} = 200$ Myr in a larger $L_{\rm box} = 500$ pc bounding box. An important assumption is that star formation in the cluster is a single-age event, and once the cluster is formed, all the gas is expelled. The core radius $r_{\rm c}$ and the concentration $c \equiv \log(r_{\rm t}/r_{\rm c})$ of the cluster, fitted by the King (1966) model, are ~ 5.7 pc and ~ 4.2, respectively.

Different models exploring physical parameters (especially those about the ambient gas properties) use the same initial condition of the fiducial model. Simulations for each model, including the fiducial model specific to the CNM, are conducted with three types of gas-star interactions, indicated as "NDF", "DF" and "None" as the suffixes of the models, to emphasize the modes of the gas-star interactions. Note that the stars that do not launch winds (e.g., WDs) always experience DF effect even in the model marked as "NDF".

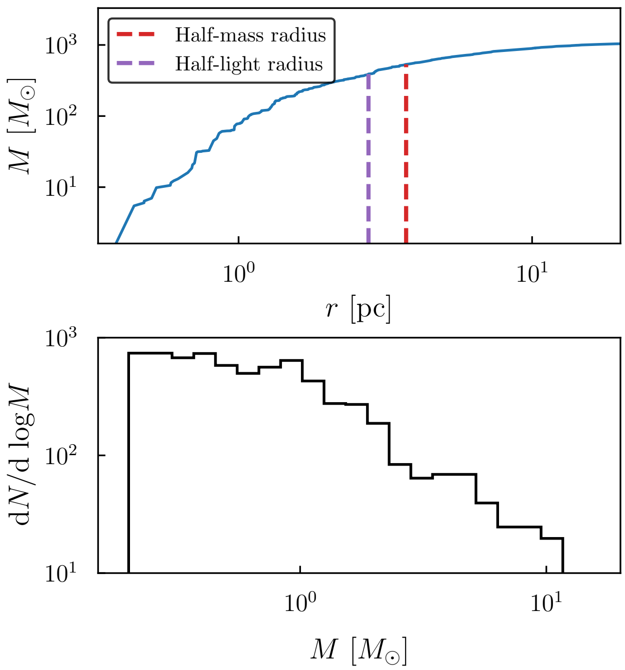

Figure 2. The initial condition of the fiducial model includes the mass distribution (top panel) and logarithmic density histograms of mass (bottom panel). The red and purple dashed lines in the top panel indicate half-mass and half-light radius, respectively.

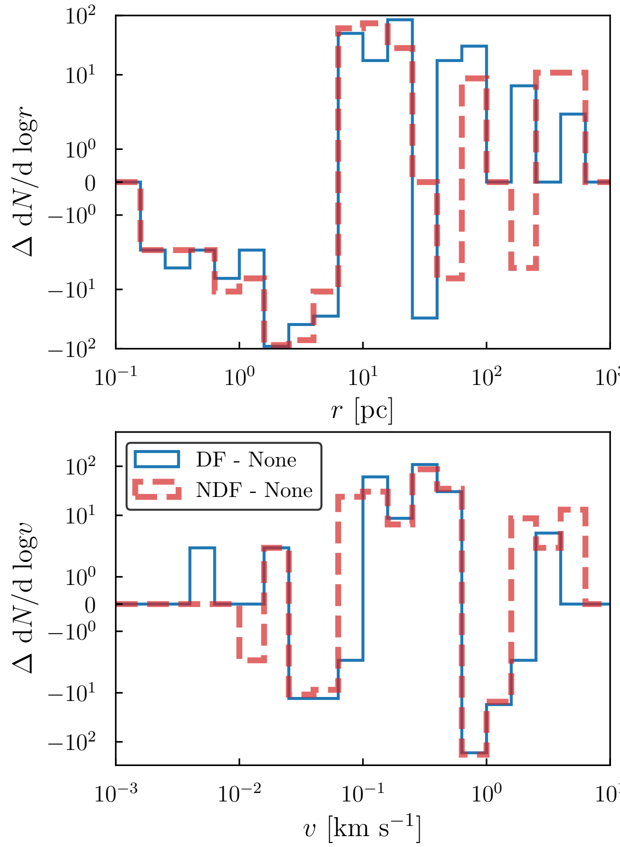

Figure 3. The differences in the distance (upper panel) and velocity (lower panel) distributions between CNMF-NDF run and CNMF-None run (red line), as well as between CNMF-DF run and CNMF-None run (blue line).

3. FIDUCIAL MODEL RESULTS

The impacts of the gas-star interactions on the model OC immersed in the fiducial uniform CNM gas ($\rho_0 = 30\ m_p\ \mathrm{cm}^{-3}$, $T = 100$ K; CNMF hereafter for this case) are illustrated by the histograms in Figures 3. Thanks to the NDF acceleration, the stars generally reside on the side with higher mechanical energy in the CNMF-NDF run, compared to its CNMF-DF and CNMF-None counterparts. The distribution of distances to the cluster center ("distances" hereafter) tilts to the more distant side, while the velocity tends to be smaller as the stars are statistically farther from the global gravitational potential minimum.

3.1. *Cluster Sizes and Velocity Dispersions*

Statistics directly related to observables are presented in Figure 4. All three models exhibit the same trend of dynamical evaporation, indicated by their increasing half-mass and half-light radii, and decreasing velocity dispersions. The half-mass radii for CNMF-NDF and CNMF-DF are both larger than the gas-free CNMF-None model by $\sim 1/3$, yet the underlying reasons should be different if one inspects the comparison in velocity dispersions. In self-gravitating systems, acceleration forces pushing the stars forward (such as NDF) tend to relocate them to shallower places in the potential well, and eventually reduces the magnitudes of velocity dispersions. Deceleration forces, in contrast, should put the stars closer to the cluster center first. However, this will lead to more frequent close encounters, which scatters stars into larger distances and also results in increased cluster sizes eventually.

Such a degeneracy in the increase of half-mass radii can also be partially resolved by the comparison in half-light radii (the middle panel of Figure 4), which weights much more on the more massive main sequence stars because of the mass-luminosity scaling relation $L \propto M^{3.5}$. After the death of the most massive stars at $t_{\mathrm{evo}} \sim 50$ Myr, the half-light radius for the CNMF-NDF model starts to considerably exceed the other two, and becomes $\sim 2\times$ as large after ~ 200 Myr. These evolution tracks imply that the increase of the cluster size for the CNMF-NDF model should be dominated by the more massive stars, whose faster and stronger stellar winds push themselves to larger distances via NDF effects. The half-light radius of the CNMF-DF model

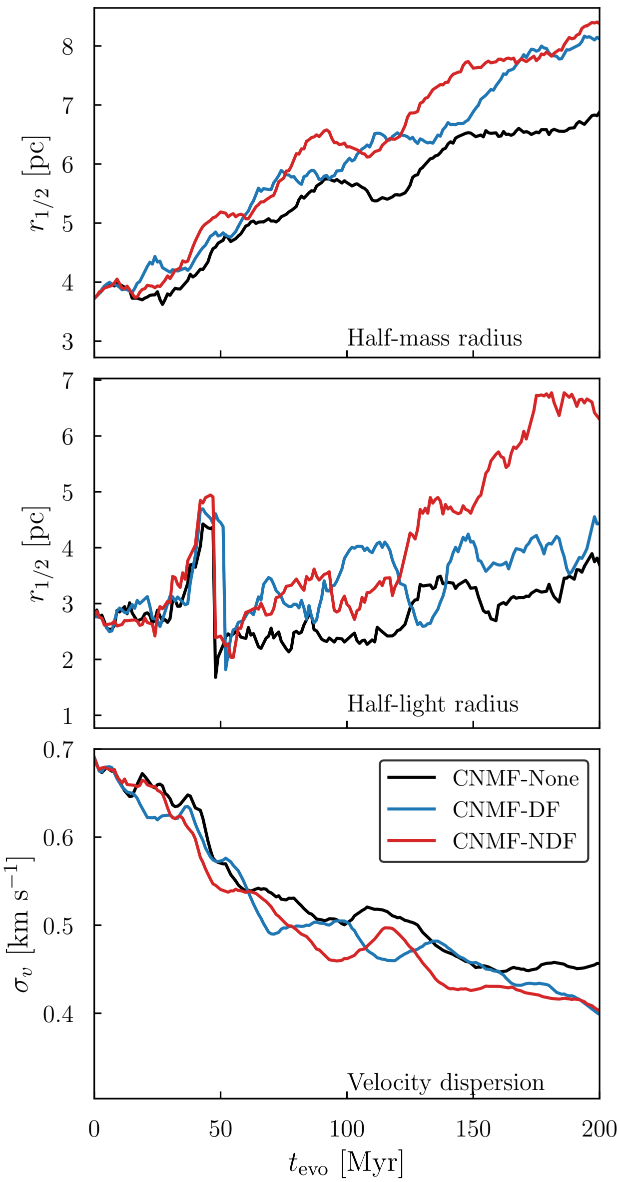

Figure 4. The half-mass radii (upper panel), half-light radii (middle panel), and velocity dispersions (lower panel) of the OC in the CNMF model during its 200 Myr evolution period. The half-light radii are calculated using the $L \propto M^{3.5}$ scaling relation for the main sequence and RGB stars, and there are "cliffs" at $t_{\rm evo} \sim 50$ Myr when the most luminous stars end their main sequence and RGB lives. Note that the statistics are calculated in three dimensions, not projected along the line of sight. When calculating the half-mass and half-light radii, the center of mass / "center of light" is determined using stars within a 100 pc range centered around the median space coordinate. Velocity dispersion is calculated based on bounded main sequence stars with negative mechanical energy in the OC's center-of-mass frame.

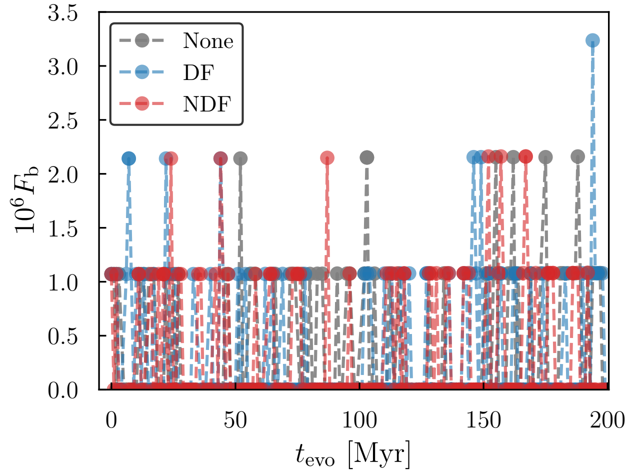

Figure 5. The evolution of bounded pairs fraction of OC for all runs in the CNMF model.

cannot catch the NDF models, since the gravitational scatterings tend to eject less massive stars due to the conservations of momentum and mechanical energy.

The formation of binaries within OC have drawn the concern in some recent research workds (e.g., Li & Mao 2018). Figure 5 illustrates the fraction of bounded pairs $F_{\rm b} \equiv N_{\rm pair,b}/N_{\rm pair,tot}$, where $N_{\rm pair,tot} = N(N-1)/2$ is the total number of pairs in the system, and $N_{\rm pair,b}$ is for the bounded pairs that have negative total energy in their center-of-mass frame. The three runs for the CNMF model does not exhibit appreciable differences in $F_{\rm b}$, as the number of stars in this work is insufficient to make the binaries important in the fiducial runs.

3.2. *Bulk Motion of Clusters*

The gas-star interactions–both NDF and DF–are the results of stellar outflows and motion. Although the CNMF model runs assume no bulk motion of the whole cluster, the realistics are usually more complicated. The centers of mass of an OC and a gas cloud can move on their own tracks when evolving in galaxies, and the relative bulk motion between the two objects should be expected. We hence introduce models CNM3 and CNM5 to study such bulk motions at center of mass speeds $v_{\rm c} = 3$ km s^{-1} and 5 km s^{-1}, respectively (see also Table 1).

Due to the morphologies of the stellar wind-ambient interaction regions, the magnitudes of NDF acceleration decreases with faster stellar velocities (Eq. 2). This relation qualitatively yields the phenomena in Figure 6, where the increase in mechanical energy caused by NDF is slightly suppressed with higher $v_{\rm c}$. Regarding the increase in half-mass and half-light radii, a similar suppression is observed in Figure 7. Concerning veloc-

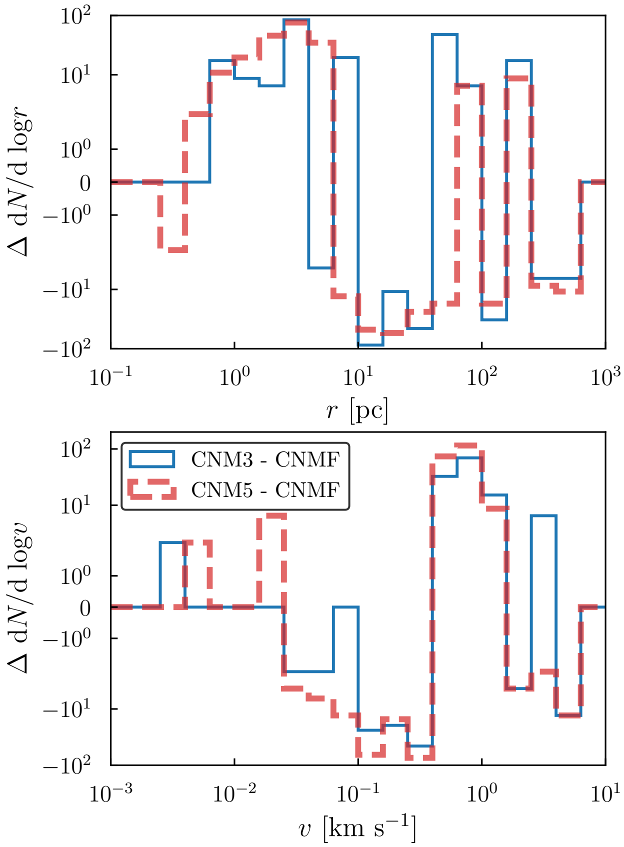

Figure 6. The differences in the distance (upper panel) and velocity (lower panel) distributions of OC with different $v_{\rm c}$ regarding CNMF after 200 Myr of evolution under the influence of NDF.

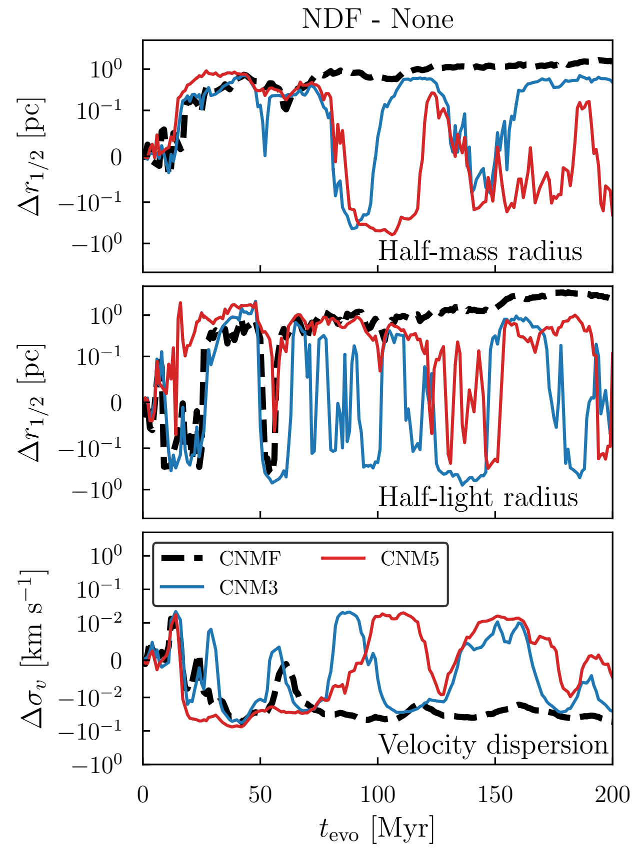

Figure 7. The evolution of the differences in half-mass radii (upper panel), half-light radii (middle panel), and velocity dispersions (lower panel) between NDF and None run across different scenarios of the fiducial model with varying $v_{\rm c}$.

ity dispersion, the suppression of NDF results in stars settling in deeper regions of the potential well, leading to larger magnitudes of velocity dispersion than the CNMF. While these patterns can be qualitatively anticipated for higher $v_{\rm c}$ velocities, detailed analyses should be based on cluster-specific calculations rather than extrapolations.

3.3. *Stellar Evolution and Compact Objects*

Outflowing stars are expected to be pushed further away from the cluster center once NDF is in action. For typical main sequence stars immersed in the CNM, however, such effects are generally obscured by the overall trend of OC dynamical evaporation. When an outflowing star travels at a small initial speed in a uniform medium, the asymptotic relation near $t \to \infty$ between the travel distance l and the time t roughly reads, using the approximate expression for Eq. (2),

$$l \sim 10 \text{ pc} \times \left(\frac{\rho}{30\ m_p\ \text{cm}^{-3}}\right)^{1/2} \left(\frac{v_{\rm w}}{400\ \text{km s}^{-1}}\right)^{1/2} \times \left(\frac{\dot{m}_{\rm w}}{10^{-13}\ M_\odot\ \text{yr}^{-1}}\right)^{1/2} \left(\frac{t}{100\ \text{Myr}}\right)^{3/2} \propto t^{3/2}\ . \tag{9}$$

In the meantime, the velocity scales as $v \propto t^{1/2}$ asymptotically. These estimations also give the *lower* limit of time required to drive a star out of the cluster even *without* the gravitational potential well. When the potential well is present, direct exclusion of a solar-mass main sequence star via NDF is not possible.

For objects with intensive outflows, however, the accelerations are much more significant dynamically. Although $a_{\rm NDF} \propto v_{\rm w}^{1/2}$ increases sub-linearly with $v_{\rm w}$, the NS with $v_{\rm w} \simeq 0.1c$ can still escape from the stellar ensemble well before the evaporation of OCs. Figure 8 illustrates the efficient expulsion of NS (upper panel) by NDF (solid lines), compared to the DF (dotted lines)

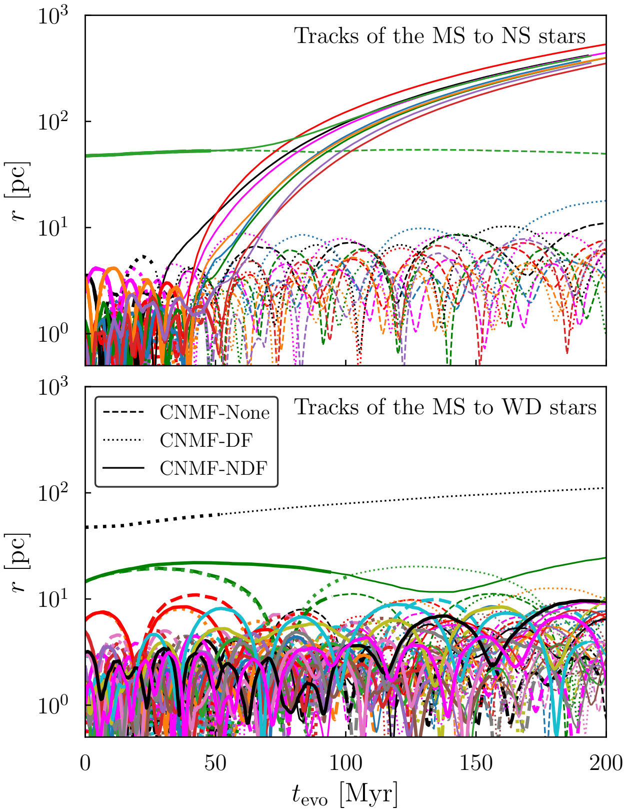

Figure 8. The evolution trajectories of stars evolving into compact objects (NS in the upper panel, and WD in the lower panel), showing the distances r to the cluster center, in CNMF with distinct stars represented by different colors. The upper and lower panels show the tracks of main sequence stars transitioning into NS and WDs under different gas-star interactions. Thick lines represent trajectories during the main sequence phase, while thin lines indicate trajectories after they evolve into NS or WD. These trajectories only depict stars exiting the main sequence within the evolution time. Note that all NSs are expelled from OC under the influence of NDF.

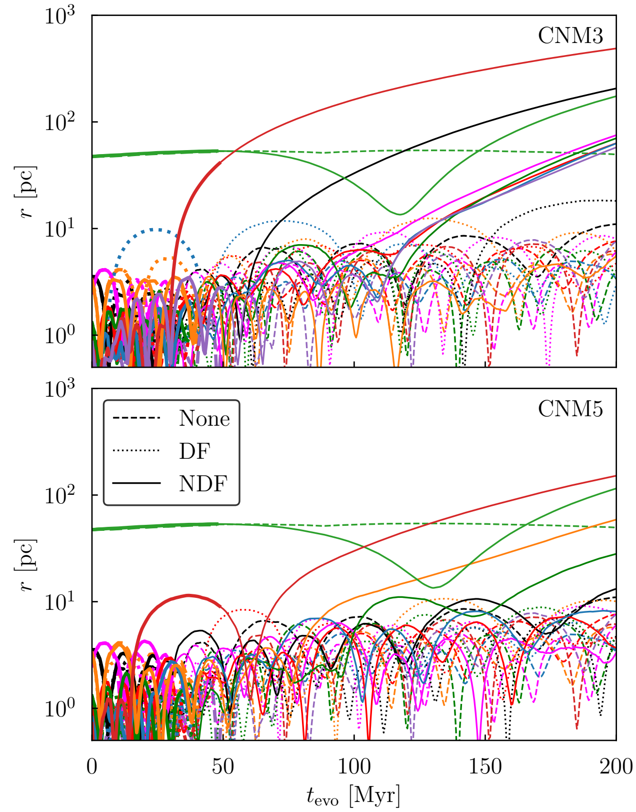

Figure 9. The evolutionary trajectories of main sequence stars transitioning into NSs are depicted in the scenarios of CNM3 (upper panel) and CNM5 (lower panel). Under the influence of NDF, main sequence stars in CNM3 move away from the OC after evolving into NSs. Within $t_{\rm evo} < 50$ Myr, a significant close encounter occurred, resulting in early expulsion during the main sequence stage for the star corresponding to the top red line. In the CNM5 scenario, only a portion of NSs have moved away, while some remain within the OC but tend to move outward.

and gas-free (dashed lines) cases where the ordinary "evaporation" process of OC is present. NS are driven out to $\gtrsim 10^2$ pc from the center of the model cluster within only ~ 50 Myr, shorter than the lifetime of a typical OC. After escaping from the OC potential, the $l \propto t^{3/2}$ scaling and Eq. (9) holds semi-quantitatively for each of the NS at large distances ($\gtrsim 10$ pc). Assuming that the gaseous disk half-thickness is ~ 0.5 kpc in the Galaxy, such expulsion process will eventually take ~ 100 Myr to remove an NS from the disk. Such quick expulsions will likely lead to the scarcity of NS in OCs, and probably in the whole gaseous galactic disk. Figure 9 illustrates a reduced expulsion of NSs attributed to the attenuation of the NDF effect by the bulk motion. The expulsion of NS is ubiquitous for gas-immersed OCs unless the cluster bulk motion is too fast relative to the gas ($\gtrsim 5$ km s^{-1}). Previous works often attribute the exclusion of NS from clusters to the "kicks" during asymmetric supernovae explosions (e.g., Fragione & Banerjee 2020). With the NDF effects, however, NS exclusion can still take place without these "kicks".

In contrast to NS, WDs do not have outflows in our model, and are not susceptible to the NDF expulsions (Figure 8, lower panel). Such model is applicable to stand-alone WDs, yet accreting WDs will likely yield accretion disk winds or even jets. In the current OC model where binaries are very rare (Figure 5), the assumption that WD have no outflows should hold reasonably well. In future works studying more stars and significantly higher occurance rate of binaries, the fate of WDs with outflows in binaries should be revisited

Table 1. Physical parameters for N-body simulations for open clusters in different scenarios.

Name	Description[†]
CNMF	Fiducial Model (Cold Neutral Media; Section 2.3)
CNM3	$v_c = 3$ km s^{-1}
CNM5	$v_c = 5$ km s^{-1}
WNM0	$[\rho] = 0$, $T = 5000$ K (Warm Neutral Media)
WNM1	$[\rho] = 1$, $T = 1000$ K (Warm Neutral Media)
MD	$[\rho] = 3$, $T = 30$ K (Diffuse Molecular Regions)
M4*	$[\rho] = 4$, $T = 30$ K (Molecular Clouds)
M5*	$[\rho] = 5$, $T = 30$ K (Molecular Clouds)
M7*	$[\rho] = 7$, $T = 30$ K (Molecular Clouds)
AGND*	$[\rho] = 9$, $T = 30$ K (AGN Disk Gases)

NOTE— †: Only the properties different from the fiducial model are described; $[\rho] \equiv \log_{10}[\rho_0/(0.3\ m_p\ \mathrm{cm}^{-3})]$
∗: Evolution time $\Delta t_{\mathrm{evo}} = 20$ Myr.

with proper modeling of their accretion feedbacks and the non-isotropic outflow patterns (e.g., Li et al. 2020).

4. MODELS EXPLORING AMBIENT GAS PROPERTIES

Although the Galaxy disk is filled with CNM predominantly (by volume), there are other phases of the interstellar media that can be encountered by an OC as it travels and evolves. We therefore conduct various simulations to study the interactions between OCs and other types of gases, including the warm neutral medium (WNM), diffuse molecular regions (MD), dense and intermediate molecular clouds, and even the midplane of active galactic nucleus (AGN) disks (Draine 2011; Cantiello et al. 2021). Properties of these gases are summarized in Table 1.

4.1. *Distributions in the Configuration and Velocity Spaces*

In a virialized self-gravitating system, stars staying at larger distances from the cluster center generally move at slower velocities. When the NDF and DF accelerations are sufficiently low and gradual, their impact on the cluster configurations is mostly adiabatic, and the system remains virialized during the evolution. When the ambient gas density is raised to $3 \times 10^8\ m_p\ \mathrm{cm}^{-3}$ in the model AGND, however, the NDF acceleration for a solar-mass star moving at 1 km s^{-1} becomes $a_{\mathrm{NDF}} \sim 10^{-9}$ cm s^{-2}, which is $\sim 10\times$ the gravitational acceleration by a $10^3\ M_\odot$ cluster at 10 pc. A cluster evolving under such strong NDF or DF accelerations no longer remains adiabatic; the dispersal takes place directly within the first ~ 5 Myr resulting in a quickly

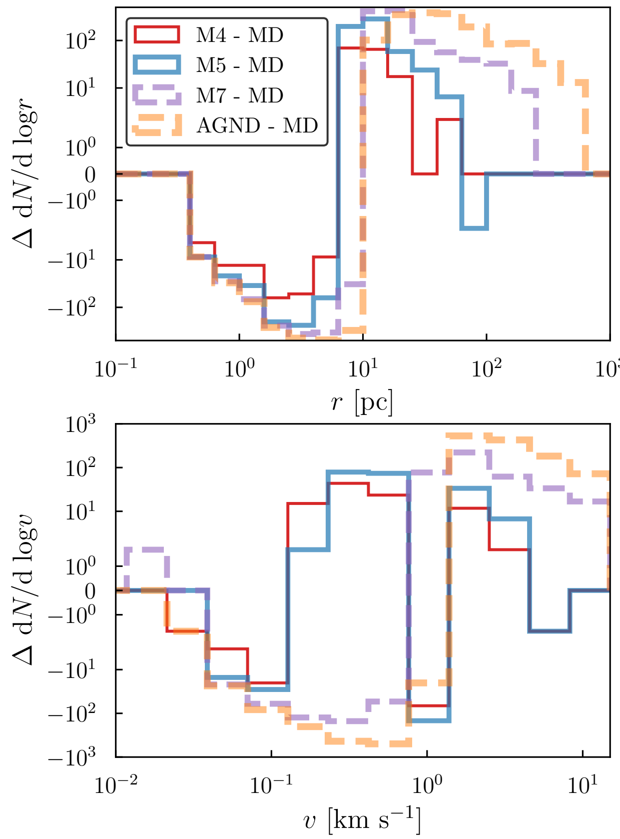

Figure 10. Similar to Figure 6, but the results shown are the difference between the labeled models and the MD (diffuse molecular regions) model (see also Table 1) for denser ambient gas without v_c, influenced by NDF.

expanding spatial size and higher velocity dispersions (Figure 11). This phenomenon also appears in the models M7 and M5 that stand for typical molecular clouds, while the models for diffuse molecular regions (model MD) and more diffuse gas (WNM0, WNM1) are qualitatively similar to the CNMF case.

Another effect that emerges in various ambient models is the stratification of stars. The acceleration by NDF on stars tend to increase their energy, which is similar to some "buoyancy" in self-gravitating OCs. As more massive stars launch more powerful stellar winds (Section 2.2), they tend to move quicker to the "surfaces" of OCs under NDF, and vice versa. Since the stellar luminosity scales as $L \propto M^{3.5}$, the half-light radii are considerably greater than half-mass radii in NDF-affected clusters. For those models that have the most dense ambients (M5, M7, AGND), the half-light radii are $\gtrsim 3\times$ greater than the half-light radii after only ~ 10 Myr, indicating an obvious radial stratification in terms of stellar types. When attempting to infer the age of an observed OC by the observations in astrometry and dynamics, one

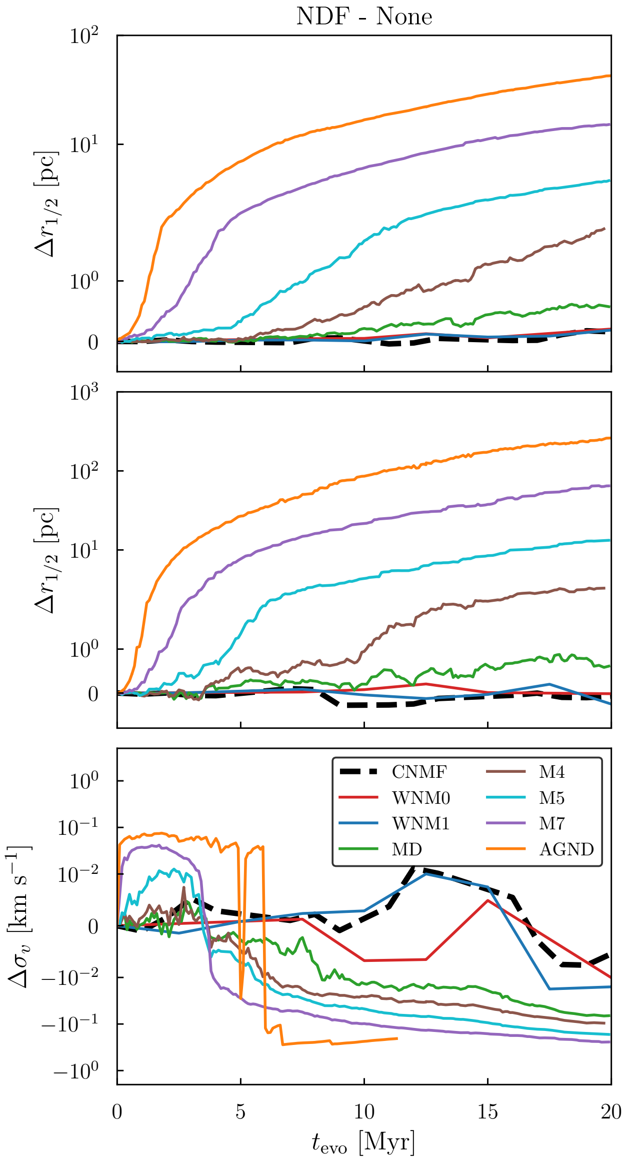

Figure 11. Similar to Figure 7, but for various ambient gas densities without $v_{\rm c}$, showing only the first 20 Myr. Note that the cut-off at around 11 Myr in the velocity dispersion of AGND exists, as no stars have negative mechanical energy in the OC's center-of-mass frame.

should take care of the possible encounters with dense clouds, whose effect in puffing up the OCs is similar to the intrinsic evaporation of clusters. Statistics on the radial distributions of mass and light in such clusters, therefore, may be helpful in reducing this type of parameter degeneracies.

4.2. *Puff-up and Dispersal of Open Clusters in Gases*

According to Eq. (2), the magnitude of NDF acceleration depends much more sensitively on ρ_0 than on T. Figure 10 reveals the general trend that the NDF effects increase with denser ambient gas, raising the total mechanical energy and easing the evaporation of cluster stars. The scaling relation in Eq. (2) is sub-linear with respect to ρ_0 ($\sim \rho_0^{1/2}$). Assuming a relatively invariant velocity distribution over the same period of time, one can infer the scaling relation $\mathrm{d}E/\mathrm{d}t \sim \rho_0^{1/2}$, and subsequently $\Delta|1/r| \sim \rho_0^{1/2}$. This pattern is qualitatively seen in Figure 11, yet we note that such simple scaling no longer applies quantitatively when there are significant increases in velocity dispersions.

Models M5 and M7 show that OCs in relatively dense ambients will quickly puff up or even disperse within ~ 20 Myr, a timescale that is comparable or even shorter than the crossing time of an OC over a dense molecular cloud. If one adopts the typical sizes ~ 20 pc of dense molecular clouds ($\rho_0 \gtrsim 10^4\ m_p$ cm^{-3}) (Cernicharo 1991; Bergin & Tafalla 2007) with an OC crossing time $\sim$ 40 Myr (assuming bulk velocity $\sim$ 0.5 km s^{-1}), Model M5 indicates that a cluster should puff up to $r_{1/2} \gtrsim 10$ pc after this crossing. A similar process will also happen for the cluster-gas encounter with a denser molecular cloud described by Model M7, even if the lifetime limits of a few Myr for these dense clouds are considered.

AGN disks are also considered as places where stars can form, which have lifetimes on the order of $10^0 - 10^3$ Myr (Marconi et al. 2004; Martini & Weinberg 2001). If a $10^3\ M_\odot$ OC forms and stays inside the AGN disk for $\gtrsim 5$ Myr, this OC should no longer be considered as a cluster anymore, even if the destruction by orbital motion shears is not taken into account. In other words, the likelihood that one can find OCs formed in AGN disks should not be significant.

4.3. *Compact Objects and Binaries*

As elaborated in Sections 3.2 and 4.1, higher stellar velocities and lower ambient gas densities suppress the NDF acceleration. In various models, the expulsion of NS via NDF behaves accordingly. Figure 12 illustrates that, even for Model WNM1 whose ambient density is merely 3 m_p cm^{-3}, such expulsion mechanism is still working, although the time required is considerably longer. This effect is, nevertheless, still more perceptible than the CNM5 case (see Figure 9). For Model WNM0, the expulsion mechanism weakened compared to WNM1, but all NSs still tend to move away from the OC.

The fraction of bounded pairs corresponding to various models does not show any considerable changes compared to the fiducial CNMF model, except for the AGND model with DF only (Figure 13). The number of bounded pairs increased drastically by $\sim 10^2$ times

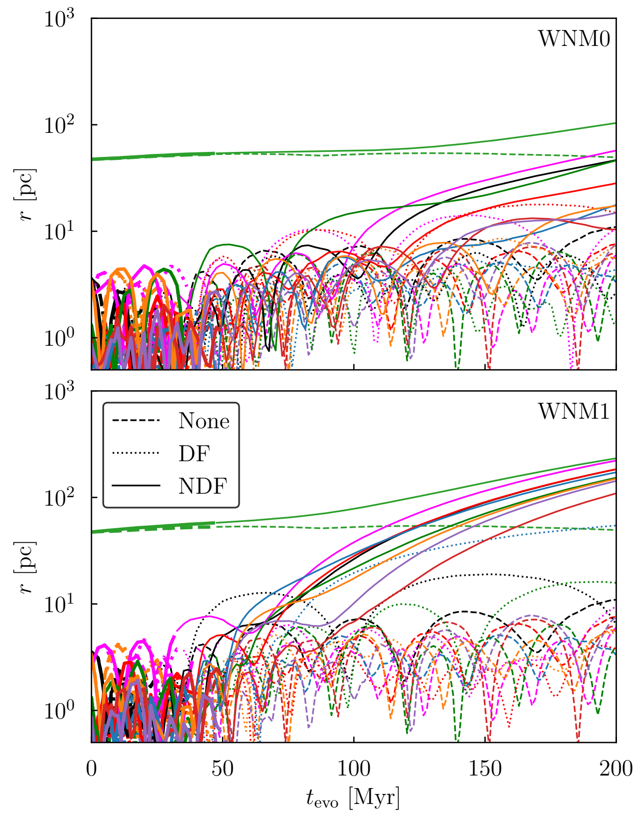

Figure 12. Similar to Figure 9, but for the scenarios of WNM0 (upper panel) and WNM1 (lower panel).

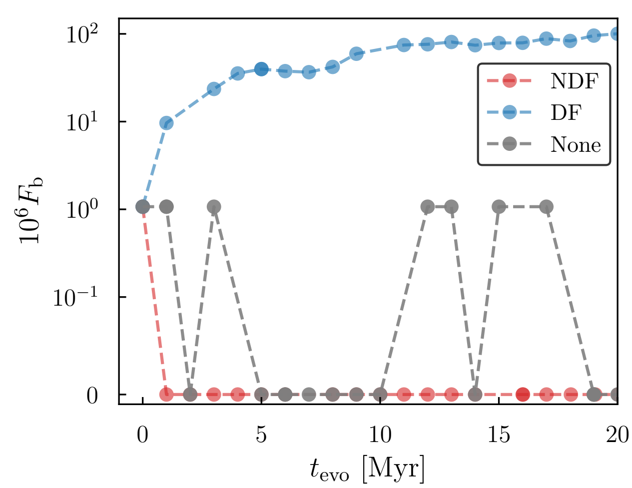

Figure 13. Similar to Figure 5, but for the AGND scenario with an evolution time of 20 Myr.

in the first $\sim$ 20 Myr of evolution. Strong deceleration caused by DF shrinks the separations between stars and reduces stellar velocities, facilitating the formation of binaries. Several studies have explored this phenomenon. Rafikov (2013, 2016) proposed that gas-assisted inspirals efficiently merge supermassive BH binaries within a Hubble time. The introducing NDF would nonetheless "flip" this scenario, widening the binary separations. Wang & Li (2022) demonstrated in simulations of AGB star-outflowing pulsars that a dense and slow outflow exerts a positive torque on the binary, causing $\gtrsim$ 10% orbit expansion. Extrapolating these mechanisms to the OCs immersed in dense gas can cause a severe inhibition of binary occurrence rates.

5. DISCUSSION AND SUMMARY

In this paper we study the evolution of OCs immersed in galactic gases. Overall, the introduction of NDF makes the OC puffier and eases the evaporation of cluster stars, resulting in reduced velocity dispersions and increased half-mass and half-light radii. This effect scales sub-linearly with the ambient density and is mostly irrelevant to the ambient temperature as the ram pressures on both sides dominate the gas-star interactions. NS with powerful winds are expelled from the cluster due to the intense NDF effect, while WD stars undergo conventional evaporation due to the absence of outflow.

5.1. *Impacts of the NDF Effects on Cluster Evolution*

While gas DF has garnered most of the attention, NDF has been relatively overlooked. Opposite to DF, NDF accelerates stars along their motion direction. Such difference in the effects between NDF versus DF can "flip" the signs of multiple physical mechanisms. For instance, one may expect that the OC evaporation is suppressed or even inhibited by DF when encountered with gas, while the actual scenario could be right the opposite due to NDF. In the densest gases including dark molecular clouds, AGN disks, and AGN tori (whose average column density is as high as $\sim 10^{24}$ cm^{-2}; see, e.g., Zhao et al. 2021), dispersal of OCs can be almost instant compared to their dynamical lifetimes as clusters. Interpretations about observations on cluster kinetics should take the possibility of NDF into account.

Observation missions like Gaia (Gaia Collaboration et al. 2016) provide abundant astrometric data for stars in our galaxy, facilitating the study of OCs' dynamical evolution (e.g., Maurya et al. 2023). Because of the radial stratification in stellar masses (Section 4.1), one can prospectively tell the effects of gas-star interactions by measuring the half-mass and half-light radii, as well as the velocity dispersions. The combination of high precision photometry with astrometry can further help the researchers to find out the radial distribution functions of different stellar types. These measurements can be a direct characterization of gas-star interaction history that are potentially important for identifying an OC's "invasion" into dense gases during its evolution history.

5.2. *Neutron Star Depletion*

Due to substantial outflows, NSs gradually drift away from their associated OC under the influence of NDF in all simulations. Conversely, WD stars influenced by NDF experience a pulse momentum injection from the main sequence to the AGB stage and subsequently to the WD stage. However, upon transitioning into the WD phase, WDs decelerate due to DF as they lack outflows. This mechanism ensures that WDs remain confined within the OC and experience conventional evaporation.

It is commonly assumed that kicks by asymmetric supernovae drive NS to high velocities relative to the cluster centers, and eventually expel them from OCs. Lai (2004) reviewed various physical mechanisms leading to kicks, and Bortolas et al. (2017) suggested that NSs are generally scattered away from SgrA* due to such kicks. Contenta et al. (2015) indicated that the natal kick of NSs can alter the star cluster's lifetime by almost a factor of ~ 4. Admittedly, the kicks serve as an effective expulsion mechanism of NS. However, kicks only entail a one-time momentum injection, whose intensity and direction of momentum injection is stochastic and can well result in the NS's deceleration. The NDF effects are, in contrast, a much more steady and robust mechanism that almost ensures the expulsion without gravitational scatterings. Such effects can further lead to the reduction of NS binaries and mergers within OCs, which is potentially relevant to the spatial distribution of NS-related mergers and gravitational wave events.

5.3. *Future Works*

Due to the limitations in physical modeling and computation, this work does have some caveats and issues that should be addressed in future works. For example, simplistic isotropic stellar wind models are adopted for each type of star, which is suitable only for a fraction of NS. Many NS–especially those with accretion disks–may launch directed or bipolar outflows, which could affect the intensity and direction of the NDF forces (Li et al. 2020). The WD model in this study lacks wind and is susceptible to DF only. While stand-alone WD stars may not have outflows, accretion from their companions may cause disk winds and jets. This study ignores the time lag in forming stars within the OC and does not consider the interaction between star and star-forming gas. However, the expulsion of residual star-forming gas does not occur instantaneously after the completion of the star formation process in actual scenario. Observations reveal that star formation efficiencies within OCs vary widely, ranging from several percent to 30 percent for dense clumps within molecular clouds (Lada & Lada 2003; Higuchi et al. 2009), and from 0.1 percent to a few percent for their associated giant molecular clouds (Evans et al. 2009; Murray 2011). This implies that newly formed or forming stars (such as protostars and pre-MS stars, which have outflows) would interact with star-forming gas, resulting in the influence of NDF on the initial phase space distribution of stars within young OC. Moreover, the stellar winds from these stars may blow unprocessed gas out of the cluster, inhibiting the ongoing star formation process. Refined models in the future should take the complexities of stellar outflows and the star formation process into account.

Although our study considers the highly dense scenario of an AGN disk (AGND scenario), we have omitted multiple physical conditions relevant to AGN in order to isolate and emphasize the impact by NDF. Incorporating the shear effect is crucial for understanding stellar formation and evolution within AGN disks. However, this topic is specific to disks and beyond the scope of this paper, which should be addressed in a separate study. Future studies on AGN disks will require additional considerations, such as orbital motion and vertical stratification of gas. The limited thickness of AGN disks differs substantially from the assumed uniform gas ambient in this paper, especially considering the vertical density gradients. Furthermore, isolated stars would experience the DF effects in the highly-dense environment of a galaxy's circumnuclear regions. Future works shall also explore these possibilities of NDF-affected stars.

In addition, our studies focus on relatively small and sparse OCs with $\sim 10^3$ stars. In high-density environments, particularly in AGN disks, super star clusters are often present instead of OCs, whose star formation efficiencies are high enough to survive as globular clusters. Investigating larger ensembles of stars such as globular clusters can impose additional challenges. Globular clusters have $\sim 10^6$ or even more stars, while each of the stars might still be dynamically important. Accurate treatments of frequent close encounters are beyond the capacity of ordinary orbital integrators with tree-based or particle-mesh based gravity solvers, and special algorithms are required for sufficient accuracy. During close encounters, shock structures caused by gas-star interactions on both sides may collide, resulting in highly complex gas morphologies and interaction patterns. Understanding how such complex physical scenarios affect the dynamical evolution of stars within globular clusters could be explored once proper algorithms are prepared for complicated computations. Even without proper treatments of frequent close encounters in more massive clusters, the dynamical evolution of compact objects (NS, WD, and BH) are still qualitatively feasible within the current framework for globular clusters and super star clusters. Detailed discussions are nontheless beyond the scope of the current paper focusing on OCs, and a subsequent paper is being composed specifically addressing this issue.

L. C. Ho was supported by the National Science Foundation of China (11991052, 12233001), the National Key R&D Program of China (2022YFF0503401), and the China Manned Space Project (CMS-CSST-2021-A04, CMS-CSST-2021-A06). X. Fu thanks the support of the National Natural Science Foundation of China (NSFC) No. 12203100 and the China Manned Space Project with NO. CMS-CSST-2021-A08. M. Liu and L. Wang appreciates the computational resources provided by the Kavli Institute of Astronomy and Astrophysics at Peking University. We also thank our colleagues Renyue Cen, Kohei Inayoshi, Fangzhou Jiang, and Meng Sun for helpful discussions and suggestions.

REFERENCES

Baruteau, C., Cuadra, J., & Lin, D. N. C. 2011, ApJ, 726, 28, doi: 10.1088/0004-637X/726/1/28

Bergin, E. A., & Tafalla, M. 2007, ARA&A, 45, 339, doi: 10.1146/annurev.astro.45.071206.100404

Bernabeu, G., Magazzu, A., & Stalio, R. 1989, A&A, 226, 215

Binney, J., & Tremaine, S. 2008, Galactic Dynamics: Second Edition

Bondi, H., & Hoyle, F. 1944, MNRAS, 104, 273, doi: 10.1093/mnras/104.5.273

Bortolas, E., Mapelli, M., & Spera, M. 2017, MNRAS, 469, 1510, doi: 10.1093/mnras/stx930

Bressan, A., Marigo, P., Girardi, L., et al. 2012, MNRAS, 427, 127, doi: 10.1111/j.1365-2966.2012.21948.x

Brooks, D. H., Ugarte-Urra, I., & Warren, H. P. 2015, Nature Communications, 6, 5947, doi: 10.1038/ncomms6947

Cantat-Gaudin, T. 2022, Universe, 8, 111, doi: 10.3390/universe8020111

Cantiello, M., Jermyn, A. S., & Lin, D. N. C. 2021, ApJ, 910, 94, doi: 10.3847/1538-4357/abdf4f

Cernicharo, J. 1991, in NATO Advanced Study Institute (ASI) Series C, Vol. 342, The Physics of Star Formation and Early Stellar Evolution, ed. C. J. Lada & N. D. Kylafis, 287, doi: 10.1007/978-94-011-3642-6_8

Chandrasekhar, S. 1943, ApJ, 97, 255, doi: 10.1086/144517

Chen, Y., Bressan, A., Girardi, L., et al. 2015, MNRAS, 452, 1068, doi: 10.1093/mnras/stv1281

Choi, J., Dotter, A., Conroy, C., et al. 2016, ApJ, 823, 102, doi: 10.3847/0004-637X/823/2/102

Contenta, F., Varri, A. L., & Heggie, D. C. 2015, MNRAS, 449, L100, doi: 10.1093/mnrasl/slv026

Demircan, O., & Kahraman, G. 1991, Ap&SS, 181, 313, doi: 10.1007/BF00639097

Draine, B. T. 2011, Physics of the Interstellar and Intergalactic Medium

Duncan, R. C., Shapiro, S. L., & Wasserman, I. 1986, ApJ, 309, 141, doi: 10.1086/164587

Edgar, R. 2004, NewAR, 48, 843, doi: 10.1016/j.newar.2004.06.001

Evans, Neal J., I., Dunham, M. M., Jørgensen, J. K., et al. 2009, ApJS, 181, 321, doi: 10.1088/0067-0049/181/2/321

Fragione, G., & Banerjee, S. 2020, ApJL, 901, L16, doi: 10.3847/2041-8213/abb671

Friel, E. D. 1995, ARA&A, 33, 381, doi: 10.1146/annurev.aa.33.090195.002121

Fu, X., Bragaglia, A., Liu, C., et al. 2022, A&A, 668, A4, doi: 10.1051/0004-6361/202243590

Gaia Collaboration, Prusti, T., de Bruijne, J. H. J., et al. 2016, A&A, 595, A1, doi: 10.1051/0004-6361/201629272

Gaia Collaboration, Brown, A. G. A., Vallenari, A., et al. 2018, A&A, 616, A1, doi: 10.1051/0004-6361/201833051

—. 2021, A&A, 649, A1, doi: 10.1051/0004-6361/202039657

Gaia Collaboration, Vallenari, A., Brown, A. G. A., et al. 2023, A&A, 674, A1, doi: 10.1051/0004-6361/202243940

Gruzinov, A., Levin, Y., & Matzner, C. D. 2020, MNRAS, 492, 2755, doi: 10.1093/mnras/staa013

Habing, H. J., & Olofsson, H. 2004, Asymptotic Giant Branch Stars (Springer-Verlag New York), doi: 10.1007/978-1-4757-3876-6

Higuchi, A. E., Kurono, Y., Saito, M., & Kawabe, R. 2009, ApJ, 705, 468, doi: 10.1088/0004-637X/705/1/468

Hoyle, F., & Lyttleton, R. A. 1939, Proceedings of the Cambridge Philosophical Society, 35, 405, doi: 10.1017/S0305004100021150

Hunt, E. L., & Reffert, S. 2023, A&A, 673, A114, doi: 10.1051/0004-6361/202346285

Just, A., Yurin, D., Makukov, M., et al. 2012, ApJ, 758, 51, doi: 10.1088/0004-637X/758/1/51

Kato, M. 1983, PASJ, 35, 33

Kim, H., & Kim, W.-T. 2007, ApJ, 665, 432, doi: 10.1086/519302

King, I. R. 1966, AJ, 71, 64, doi: 10.1086/109857

Krause, M. G. H., Offner, S. S. R., Charbonnel, C., et al. 2020, SSRv, 216, 64, doi: 10.1007/s11214-020-00689-4

Kroupa, P. 2002, Science, 295, 82, doi: 10.1126/science.1067524

Krumholz, M. R., McKee, C. F., & Bland-Hawthorn, J. 2019, ARA&A, 57, 227, doi: 10.1146/annurev-astro-091918-104430

Kudritzki, R. P., & Reimers, D. 1978, A&A, 70, 227

Kuiper, G. P. 1938, ApJ, 88, 472, doi: 10.1086/143999

Lada, C. J., & Lada, E. A. 2003, ARA&A, 41, 57, doi: 10.1146/annurev.astro.41.011802.094844

Lai, D. 2004, in Cosmic explosions in three dimensions, ed. P. Höflich, P. Kumar, & J. C. Wheeler, 276, doi: 10.48550/arXiv.astro-ph/0312542

Li, X., Chang, P., Levin, Y., Matzner, C. D., & Armitage, P. J. 2020, MNRAS, 494, 2327, doi: 10.1093/mnras/staa900

Li, Z., & Mao, C. 2018, ApJ, 859, 36, doi: 10.3847/1538-4357/aabc09

Magrini, L., Viscasillas Vázquez, C., Spina, L., et al. 2023, A&A, 669, A119, doi: 10.1051/0004-6361/202244957

Marconi, A., Risaliti, G., Gilli, R., et al. 2004, MNRAS, 351, 169, doi: 10.1111/j.1365-2966.2004.07765.x

Martini, P., & Weinberg, D. H. 2001, ApJ, 547, 12, doi: 10.1086/318331

Maurya, J., Joshi, Y. C., Samal, M. R., Rawat, V., & Gour, A. S. 2023, Journal of Astrophysics and Astronomy, 44, 71, doi: 10.1007/s12036-023-09959-3

Miville-Deschênes, M.-A., Murray, N., & Lee, E. J. 2017, ApJ, 834, 57, doi: 10.3847/1538-4357/834/1/57

Mor, R., Livne, E., & Piran, T. 2023, MNRAS, 518, 623, doi: 10.1093/mnras/stac2775

Murray, N. 2011, ApJ, 729, 133, doi: 10.1088/0004-637X/729/2/133

Ostriker, E. C. 1999, ApJ, 513, 252, doi: 10.1086/306858

Paczynski, B. 1990, ApJ, 363, 218, doi: 10.1086/169332

Pang, X., Tang, S.-Y., Li, Y., et al. 2022, ApJ, 931, 156, doi: 10.3847/1538-4357/ac674e

Portegies Zwart, S. F., McMillan, S. L. W., & Gieles, M. 2010, ARA&A, 48, 431, doi: 10.1146/annurev-astro-081309-130834

Rafikov, R. R. 2013, ApJ, 774, 144, doi: 10.1088/0004-637X/774/2/144

—. 2016, ApJ, 827, 111, doi: 10.3847/0004-637X/827/2/111

Ramstedt, S., Schöier, F. L., Olofsson, H., & Lundgren, A. A. 2008, A&A, 487, 645, doi: 10.1051/0004-6361:20078876

Rein, H., & Liu, S. F. 2012, A&A, 537, A128, doi: 10.1051/0004-6361/201118085

Rein, H., & Spiegel, D. S. 2015, MNRAS, 446, 1424, doi: 10.1093/mnras/stu2164

Salpeter, E. E., & Shapiro, S. L. 1981, ApJ, 251, 311, doi: 10.1086/159466

Sandage, A. R. 1953, AJ, 58, 61, doi: 10.1086/106822

Solomon, P. M., Rivolo, A. R., Barrett, J., & Yahil, A. 1987, ApJ, 319, 730, doi: 10.1086/165493

Sun, J., Leroy, A. K., Schruba, A., et al. 2018, ApJ, 860, 172, doi: 10.3847/1538-4357/aac326

Tagawa, H., Haiman, Z., & Kocsis, B. 2020, ApJ, 898, 25, doi: 10.3847/1538-4357/ab9b8c

Tanaka, H., Takeuchi, T., & Ward, W. R. 2002, ApJ, 565, 1257, doi: 10.1086/324713

Tang, J., Bressan, A., Rosenfield, P., et al. 2014, MNRAS, 445, 4287, doi: 10.1093/mnras/stu2029

Tarricq, Y., Soubiran, C., Casamiquela, L., et al. 2022, A&A, 659, A59, doi: 10.1051/0004-6361/202142186

—. 2021, A&A, 647, A19, doi: 10.1051/0004-6361/202039388

Wang, L., & Li, X. 2022, ApJ, 932, 108, doi: 10.3847/1538-4357/ac6ce6

Zhao, X., Marchesi, S., Ajello, M., et al. 2021, A&A, 650, A57, doi: 10.1051/0004-6361/202140297